Available online at www.sciencedirect.com

ScienceDirect

Energy Procedia 92 (2016) 590 – 599

Energy Procedia

6th International Conference on Silicon Photovoltaics, SiliconPV 2016

Anti-reflective coated glass and its impact on bifacial modules' temperature in desert locations

Jorge Rabanal-Arabach[a*], Andreas Schneider[a]

[a] *International Solar Energy Research Center (ISC), Rudolf-Diesel-Str. 15, 78467 Konstanz, Germany*

Abstract

Without any doubt does anti-reflective coating (ARC) on solar glass help to boost the annual module performance in the range of 3 to 4% for monofacial modules with Sunarc AR coated glass under moderate climate conditions [1] which certainly differ from desert climates. In this work three bifacial and one monofacial photovoltaic modules, with different glass coatings, are installed in a desert region as the Atacama Desert in Chile, with the optimum tilt for the location and same surrounding conditions. From the results it is observed that the glass/glass bifacial modules with ARC on both glass sheets can achieve a mean performance ratio (PR) of up to 5% higher than a module without coating in any of both glasses. It is also observed that the thermal dependence of PR for modules with ARC on both glasses and its operative temperature are larger compared to modules without coated glass.

© 2016 The Authors. Published by Elsevier Ltd. This is an open access article under the CC BY-NC-ND license (http://creativecommons.org/licenses/by-nc-nd/4.0/).
Peer review by the scientific conference committee of SiliconPV 2016 under responsibility of PSE AG.

Keywords: Photovoltaic module; anti-reflective coating; outdoor measurements; module temperature; performance ratio.

1. Introduction

In a photovoltaic (PV) system, the solar irradiance doses and the module operating temperature are the most important factors for energy yield. For bifacial PV systems, albedo is another important factor [2-4]. For high albedo higher energy yield is expected. The term albedo (Latin for white) is defined as the ratio of the reflected light by a surface compared to that received by it. In [5], J. A. Coakley constructed a global map of the diurnally averaged surface albedo for winter and summer solstice conditions, under cloud-free skies. It is clear that desert locations have an albedo in the range of 25 to 40%, and it is estimated to be seasonal invariant. These computations match with the visual experience and measurements performed by the authors in the Atacama Desert in Chile. The authors measured a modal albedo of approximately 25% in winter, for a 30° tilted installation using a CMA11 albedometer of spectral range (50% points) between 285 to 2800 nm.

1876-6102 © 2016 The Authors. Published by Elsevier Ltd. This is an open access article under the CC BY-NC-ND license (http://creativecommons.org/licenses/by-nc-nd/4.0/).
Peer review by the scientific conference committee of SiliconPV 2016 under responsibility of PSE AG.
doi:10.1016/j.egypro.2016.07.024

Nomenclature

ρ	ribbon conductivity (Ω mm^2 m^{-1})
b	cell spacing (m)
E_{DC}	direct current energy (W h)
G	global in-plane irradiance (W m^{-2})
G_b	net global in-plane irradiance (W m^{-2})
G_{STC}	global in-plane irradiance at standard test conditions (1000 W m^{-2})
H	global in-plane irradiation (W h m^{-2})
H_b	net global in-plane irradiation (W h m^{-2})
I	electrical current (A)
I_{MPP}/G_b	ratio between output current at maximum power point and net global in-plane irradiance (mA W^{-1} m^2)
I_{SC}/G	ratio between short circuit current and global in-plane irradiance (mA W^{-1} m2)
I_{SC}/G_b	ratio between short circuit current and net global in-plane irradiance (mA W^{-1} m^2)
L	cell length (m)
n_{busbar}	amount of busbar per cell
P	power (W)
P_{norm}	normalized power
t	ribbon thickness (mm)
T_a	ambient temperature (K)
T_m	module temperature (K)
V	voltage (V)
w	ribbon width (mm)
Y_A	Module energy yield (W h W$_P^{-1}$)
Y_R	Reference energy yield

1.1. Effective albedo

The ground albedo spectrum depends on the land material composition. Although the spectral-integrated value falls in the same range for several different materials, diverse ground composition not necessarily affect in the same way to the PV system under evaluation. Therefore the spectral response for different albedos depends on ground and solar cell materials [6]. M.P. Brennan et al. in [7] proposed an index called effective albedo, for different PV cell technologies and several surface reflectivities. The authors show that for desert areas the infrared (IR) wavelengths have an important contribution to the albedo spectrum, specifically with sandstone, which is mainly found in desert places as the Atacama Desert, Chile. The effective albedo for monocrystalline silicon (c-Si or mono-Si) is estimated to be approx. 0.63, which is close to the index estimated for polycrystalline silicon (p-Si, mc-Si or poly-Si). Fig. 1 plots (a) the reflectance for different ground materials as sandstone, concrete construction and green grass, and (b) the evaluated spectral albedo response of each material under an estimated solar spectrum for the Atacama Desert.

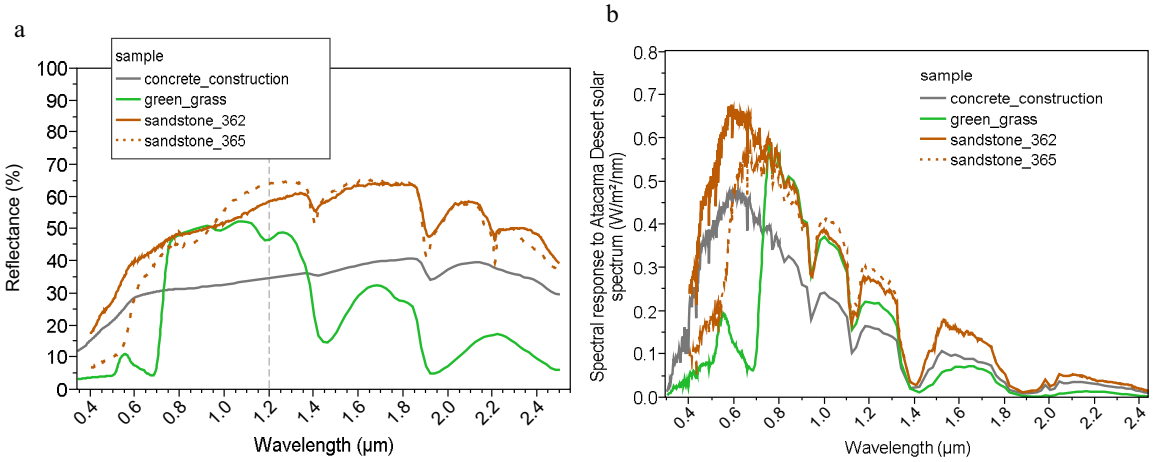

Fig. 1. (a) Example of directional hemispherical reflectance measured and catalogued in the ASTER Spectral Library [8]; (b) spectral response of samples computed under the estimated Atacama Desert solar spectrum distribution.

1.2. IR heat source

A study performed by Malte R. Vogt et al. [9] quantifies the heating contribution due to the IR from the solar spectrum on a monofacial c-Si module. Vogt and her team applied ray tracing simulation on a module assembled with 3.2 mm flat glass with an anti-reflective coating (ARC), 450 μm EVA (ethyl vinyl acetate) as encapsulant and white backsheet. Their study shows that if the IR from the standard solar spectrum AM 1.5g (approx. 20% contribution to the irradiance for wavelengths above 1200 nm) is rejected prior to entering the module then it could be possible to reduce the module temperature by 4.2% at 25°C ambient temperature and 1000 Wm^{-2}. This translates to a 19.53% drop in the temperature difference between the module and the ambient ($T_m - T_a$ from 21.5 K to 17.3 K).

However, crystalline silicon solar cells are almost transparent for wavelengths above 1200 nm. The same is valid for the module materials hence for the whole sandwich. This argument is true regardless if the light originates from the sky or is reflected from the ground. If we assume a bifacial PV module we can expect an important source of heating from the ground, especially for sandstone and white sand which have high IR contribution as it is seen in Fig. 1. For modules with ARC glass which itself does not reject the IR wavelengths (ARC_1), higher module temperatures are expected compared to modules without ARC glass (nonARC). Lower module temperatures are expected if the ARC material is able to reject part of the reflected IR (ARC_2) (see Fig. 2).

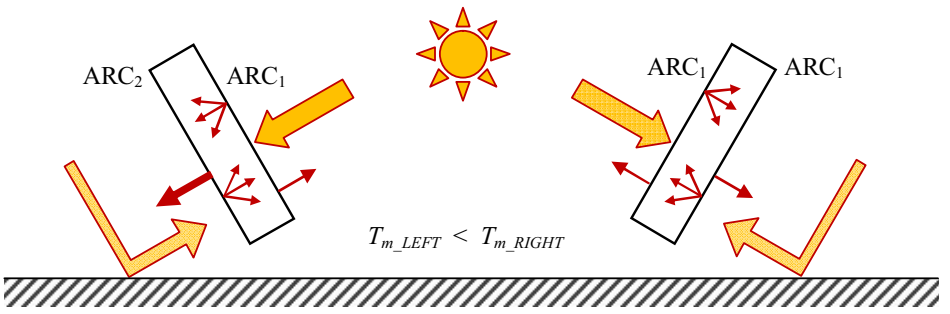

Fig. 2. Schematic view for the interaction between IR albedo and PV modules with different ARC glass.

The aim of this work is to investigate the yield performance and temperature behavior of bifacial PV modules with anti-reflective coated glass in desert locations.

2. Methodology

The aim of this work is divided in two stages. The first stage corresponds to data collection and analysis of the electrical parameters of four PV modules during 100 days from September to December 2015. Later, the second stage investigates the influence of the ground reflection on module temperature and electrical performance. Hence the ground conditions are exchanged from "normal" to "white" using a white cloth cover, collecting the data for a week.

I-V curves are measured on a regular interval and their mean values over a lapse of one minute are stored. To calculate the modules performances, short circuit current (I_{SC}), open circuit voltage (V_{OC}), current and voltage at maximum power point (MPP) (I_{MPP} and V_{MPP} respectively), the front and rear global in-plane irradiance, and the module and ambient temperatures (T_m and T_a respectively) are used. A pair of ISET irradiance sensors is used to measure the global in-plane irradiances on the front and rear surface. The net global in-plane irradiance (G_b) is obtained from the simple sum of irradiance from both sides.

2.1. Devices under test

Three bifacial and one monofacial PV modules, with different glass coatings, are installed in a non-polar desert region as Atacama Desert in Chile; facing the equator and mounted at 1.2 m height (from the ground to the lower module edge), with the same elevation-tilt (20°) and under similar surrounding conditions (mean albedo under the module of approx. 20%). These devices under test (DUT) are summarized in Table 1. All modules are manufactured with 60 bifacial solar cells (6 in. semi-square, n-type c-Si, 3 busbars and 19% efficiency), with 3 mm space from cell to cell, embedded within same kind of EVA, and interconnected with similar ribbons (1.5 mm width, 0.20 mm thick and approx. 1.54 $\Omega mm^2 m^{-1}$ electrical resistivity), junction box with 3 bypass diodes, connectors and cables. All modules are characterized indoor using an A+A+A+ sun simulator.

Table 1. Characteristics for the devices under test (DUT).

DUT	Module type	Front side	Rear side
B00	Bifacial	Solar glass	Solar glass
B11	Bifacial	Solar glass with ARC_1	Solar glass with ARC_1
B12	Bifacial	Solar glass with ARC_1	Solar glass with ARC_2
M1W	Monofacial	Solar glass with ARC_1	White backsheet

The solar glass without ARC (nonARC) and with ARC_1, and the white backsheet were characterized with in-home spectral measurements of total direct transmittance and reflectance, shown in Fig. 3. The ARC_1 glass has up to 1.88% higher transmittance and 17.5% less reflectance in the IR than the solar glass without the coating. Because of the specific physical structure of the ARC_2 layer coating, the existing spectrometer setup doesn't allow to determine the transmittance and reflectance values over the wavelengths with certain accuracy. For this reason, data for ARC_2 is missing in Fig. 3.

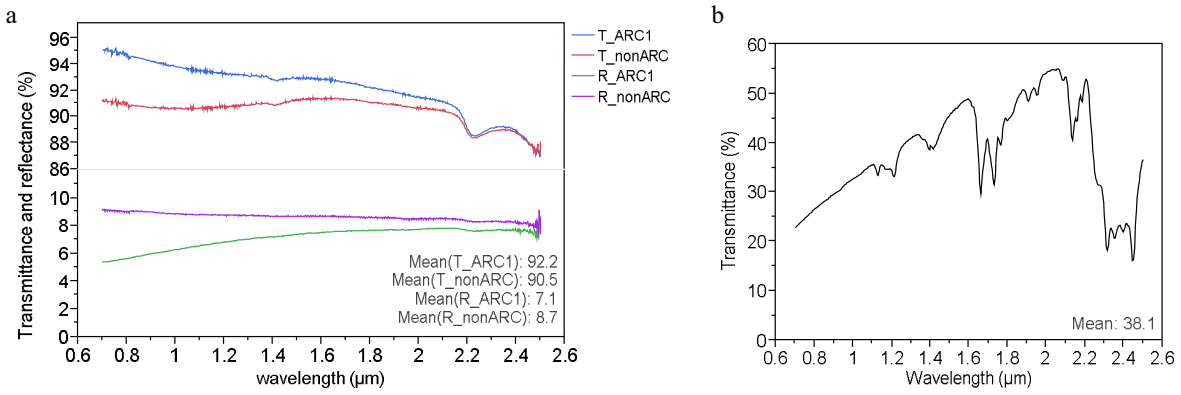

Fig. 3. a) Total direct transmittance (T_ARC1, T_nonARC) and total direct reflectance (R_ARC1, R_nonARC) in the IR section for the solar glass tested with and without ARC_1 respectively; b) total direct transmittance in the IR wavelengths for the white backsheet.

2.2. Parameters for performance evaluation

In order to evaluate the performance of a PV system, the performance ratio (*PR*) is calculated as the ratio between the daily module yield (Y_A) and the daily reference yield (Y_R) for each module (IEC-61724) [10, 11].

$$Y_A = \frac{E_{DC}}{P_{STC}} \tag{1}$$

$$Y_R = \frac{H}{G_{STC}} \tag{2}$$

$$PR = \frac{Y_A}{Y_R} = \frac{E_{DC}}{P_{STC}} \frac{G_{STC}}{H} \tag{3}$$

Where E_{DC} is the generated electrical energy (in W h), H is the global in-plane irradiation (in W h m^{-2}), and P_{STC} is the measured power of the front module side (in W) at G_{STC} irradiance (1000 W m^{-2}) at 25 °C module temperature. If the MPP power output (P_{MPP}) and frontal in-plane irradiance (G) are used in (1) - (3) instead of E_{DC} and H respectively, then the results are referred to instantaneous yields (y_A, y_R) and consequently instantaneous performance ratio (*pr*). Here, y_A stands for the so called normalized power output (P_{norm}).

The net performance ratio (PR_b) is calculated with the proviso that H in equation (3) is replaced by the net global in-plane irradiation (H_b), which is obtained from the addition of the rear irradiances contribution into H.

$$PR_b = \frac{E_{DC}}{P_{STC}} \frac{G_{STC}}{H_b} \tag{4}$$

Electrical power losses ($P_{loss.electr}$) are calculated using the equations introduced by D.H. Neuhaus et al. [12] and Ingrid Haedrich et al. [13] with the inclusion of the ribbons resistivity and dimensional change driven by the module temperature as given in [14].

$$P_{loss.ribbon} = \frac{\rho}{n_{busbar} \cdot w \cdot t} \frac{2 \cdot L}{3} I_{MPP}^2 \tag{5}$$

$$P_{loss.spacing} = \frac{\rho}{n_{busbar} \cdot w \cdot t} b \cdot I_{MPP}^2 \quad (6)$$

$$P_{loss.electr} = P_{loss.ribbon} + P_{loss.spacing} \quad (7)$$

$P_{loss.ribbon}$ estimates the power loss based on the electrical resistance for the soldered ribbons and the output current (I_{MPP}). $P_{loss.spacing}$ is the power loss due to additional electrical resistances from the spacing b (in m) between cells. The values ρ, w and t correspond to the electrical resistivity of the ribbon (in $\Omega\,mm^2\,m^{-1}$), the ribbon width (in mm), and the ribbon thickness (in mm) respectively; whilst n_{busbar} stands for the number of busbar in the solar cell and L for the cell length in the direction of the busbar (in m). The change in ribbon characteristics (ρ, w, t) due to temperature effects are calculated based on linear interpolation from experimental measurements [14].

3. Field study results

Fig. 4 summarizes the field results of the DUT. The normalized power output (P_{norm}) has a linear correlation with the in-plane irradiance (Fig. 4(a)). High irradiance implies high current and therefore the electrical power loss ($P_{loss.electr}$) increases. Further a rise in the module temperature results in a net output voltage drop (Fig. 4(b)). It remains still unclear if the electrical power loss ($P_{loss.electr}$) is the main driver for the increase in module temperature. High P_{norm} implies high I_{SC} but not necessary high voltage drop.

From Table 2, the highest maximum module temperature is observed for the bifacial module with ARC_1/ARC_1 (B11), closely followed by the monofacial one (M1W) which has ARC_1 on top (5.1%$_{rel}$, meaning a delta of 3.1 K). The modal operational module temperature is 4.9%$_{rel}$ higher for the B11 module compared to the M1W. Even when B12 has an operational temperature comparable to B00, it has a mean PR of up to 5%$_{abs}$ higher than B00.

It is also interesting to note that M1W shows the highest P_{STC} (1.8%$_{rel}$ higher than B12) but not the highest PR (~19%$_{abs}$ lower than B12) mainly due to the rear contribution in the bifacial module. These results are in concordance with the recommendation expressed by J. Prakash Singh et al. in [15].

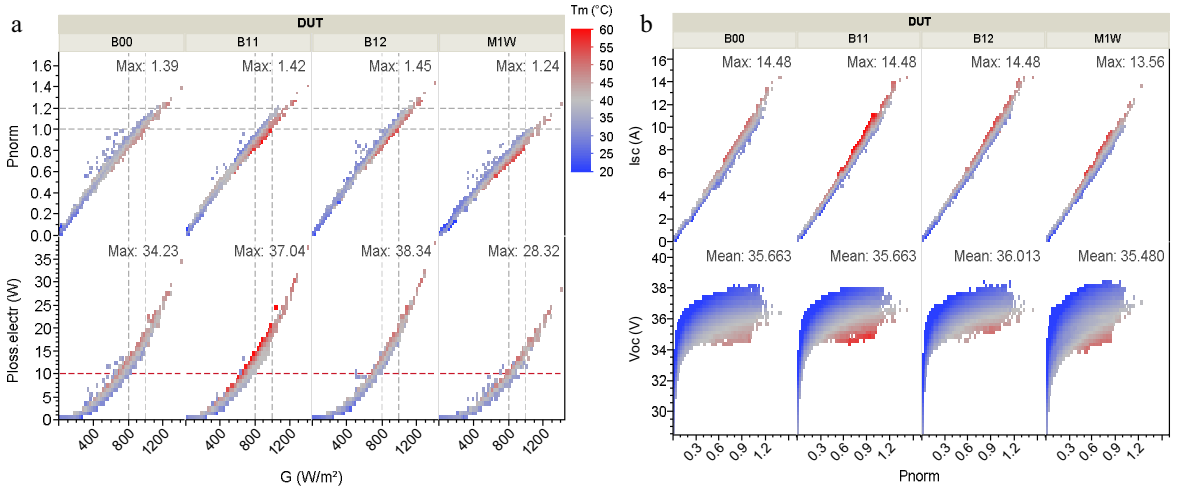

Fig. 4. Heat map for: (a) normalized power output (P_{norm}) and electrical losses ($P_{loss.electr}$) plotted versus in-plane irradiance, G; (b) short circuit current and open circuit voltage plotted versus normalized power. The same heat map gradient is employed in each graph.

Table 2. For measurements recorded during the first stage period: mean of maximum module temperature per day (max. T_m), modal module temperature (mod. T_m), mean daily performance ratio (PR) and mean daily bifacial performance ratio (PR_b). PR and PR_b are given with their respective mean, minimum and maximum values.

DUT	Front / Rear structure	Max. T_m (°C)	Mod. T_m (°C)	PR (%)	PR_b (%)
B00	nonARC / nonARC	54.0 ±0.6	42.0	107^{+8}_{-9}	89^{+7}_{-9}
B11	ARC_1 / ARC_1	63.3 ±0.3	45.2	111^{+10}_{-11}	91^{+10}_{-2}
B12	ARC_1 / ARC_2	55.9 ±0.5	41.4	112^{+14}_{-12}	94^{+6}_{-3}
M1W	ARC_1 / White_backsheet	60.2 ±0.1	43.1	93^{+7}_{-4}	77^{+7}_{-5}

ARC_1 doesn't reject IR wavelengths and also increases the internal reflection. Hence, it is expected for this module type to reach temperatures higher than a module without this ARC (nonARC), as observed for B11 and B00. B12 is a module with ARC_2 glass which is able to block part of the IR wavelengths, thereby showing a lower module temperature when compared with B11.

3.1. Comparison of a hot vs. a cold day

The hottest and the coldest day are selected and the module performance is compared. The maximum mean ambient temperature recorded (T_a) is 46°C, and the minimum is 23°C. Table 3 summarizes the module performance for the hottest and coldest day recorded. B11 has the highest thermal difference (between cold and hot days) of $50\%_{rel}$ and the largest drop in PR, by $9.4\%_{abs}$. It is also found that the thermal dependence of PR ($\Delta PR / \Delta T_m$) is higher for B11 than for B00. Interestingly, the data analysis (V_{OC} vs T_m performed at G levels between 950 to 1050 Wm^{-2}) shows a difference in voltage thermal coefficient ($\Delta V_{OC} / \Delta T_m$) between B00 and B11. This can be explained due to the increase in photon flux concentration which would result in a low voltage thermal coefficient [16], probably due to the presence of the ARC layers on the glass used in this work.

Table 3. Module performance for the hottest and coldest day recorded. The maximum net temperature (Max. ($T_m - T_a$)), the daily performance ratio (PR), the PR thermal coefficient ($\Delta PR / \Delta T_m$) and the voltage thermal coefficient ($\Delta V_{OC} / \Delta T_m$) are displayed.

		Max.($T_m - T_a$) (K)		PR (%)		$\Delta PR / \Delta T_m$	$\Delta V_{OC} / \Delta T_m$
DUT	Front / Rear structure	Hot day	Cold day	Hot day	Cold day	(1/K)	(1/K)
B00	nonARC / nonARC	10.3	7.5	108.1	114.8	−0.26	$-3.30 \cdot 10^{-3}$
B11	ARC_1 / ARC_1	18.9	9.5	108.2	117.6	−0.29	$-2.67 \cdot 10^{-3}$

3.2. Stage 2: White ground experiment

The ground albedo for modules B00 and B11 are exchanged from "normal" to "white", increasing the measured albedo from approx. 20% to 35%. From Fig. 5(a), at a given G the average net temperature ($T_m - T_a$) decreases for white ground, thus a lower voltage drop and higher P_{norm}, although $P_{loss.electr}$ increases. Nevertheless, even when the albedo increases by approx. $75\%_{rel}$ the P_{MPP} increases only by $9.8\%_{rel}$ and $9.5\%_{rel}$ respectively. This phenomenon can be attributed to a high module series resistance as discussed in [17]. I_{SC} cannot be considered linearly proportional to the net global in-plane irradiance due to the high series resistance. This is further elaborated in Fig. 5(b), where the ratios of $I_{SC} : G_b$ and $I_{MPP} : G_b$ should remain constant between the two different ground conditions, but drops due to the high modules' series resistance.

The increment in albedo from 20% to 35% implies an increment in yield (Y_A) of 6.7%$_{rel}$ and 5.6%$_{rel}$ for B00 and B11 modules respectively (see Table 4). It seems logical to condition the ground to a white albedo for nonARC glass modules (B00) than for modules with ARC glass (B11). This experiment also reveals that the electrical power losses are not the main module temperature driver but the ground reflected IR irradiation has a significant contribution to T_m. Nevertheless, even if part of the IR is avoided, the benefit in terms of electrical power is not directly proportional due to the large series electrical losses. Thus, these results prove the electrical losses to be responsible for limiting the module power output and complement previous discussions in [17-20].

Table 4. The measured daily energy yield (Y_A), performance ratio (PR) and net module temperature ($T_m - T_a$), for the two evaluated grounds.

	Y_A (Wh/Wp)		PR (%)		Max($P_{loss.electr}$) (W)		Mean(Max($T_m - T_a$)) (K)		Mean($T_m - T_a$) (K)	
DUT	normal	white	normal	white	normal	white	normal	white	normal	white
B00	6.55 ±0.50	6.99 ±0.12	109.6 ±0.0	121.4 ±0.2	14.76	16.43	14.3 ±1.0	9.2 ±0.8	5.9 ±0.8	4.4 ±0.5
B11	6.74 ±0.48	7.12 ±0.1	112.8 ±0.0	123.7 ±0.1	16.15	18.75	18.7 ±1.3	12.1 ±1.5	8.3 ±0.7	6.0 ±0.9

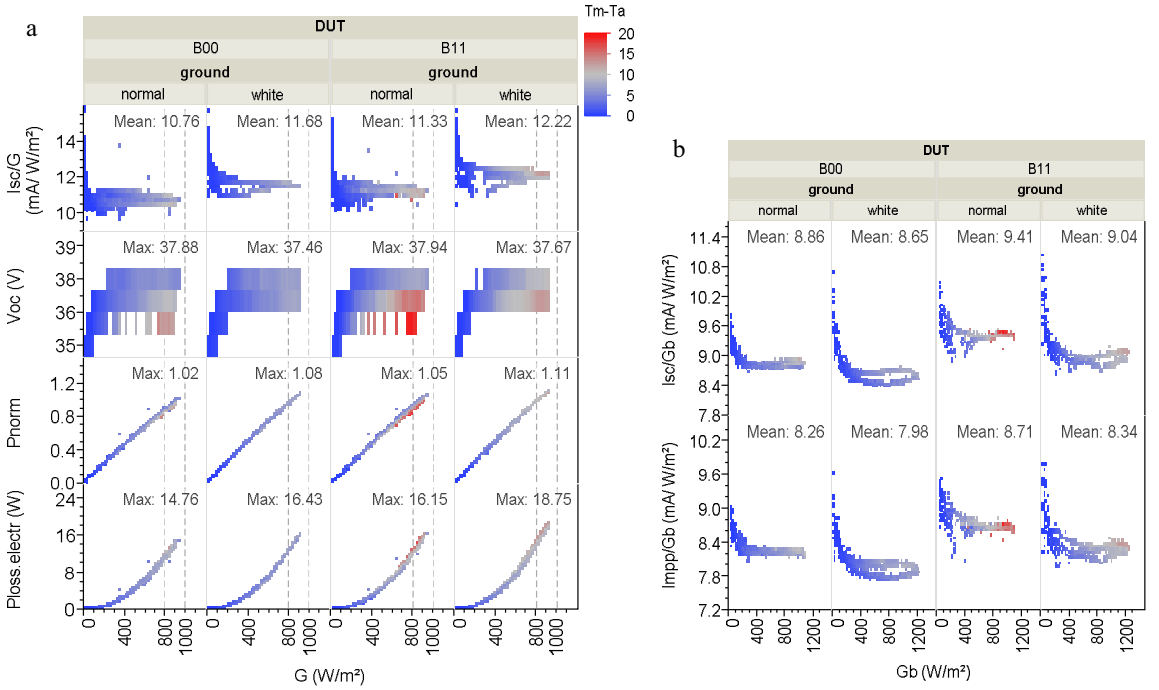

Fig. 5. Heat map for: (a) the I_{SC} : G ratio, open circuit voltage (V_{OC}), normalized power (P_{norm}) and electrical losses ($P_{loss.electr}$) for normal and white ground, plotted versus the global in-plane irradiance (G); (b) the I_{SC} : G_b and I_{MPP} : G_b ratios plotted versus G_b. The same heat map gradient is employed in each graph.

4. Conclusion

The results indicate that the bifacial module without ARC (B00) obtained a PR of up to 15%$_{rel}$ higher than the monofacial module with ARC$_1$ glass (M1W). In similar way, the glass/glass bifacial modules with ARC on both glass sheets achieved a performance ratio (PR) of up to 5%$_{abs}$ higher than modules without ARC on any of both glasses, with an operating temperature difference of approx. 3.2 K. If part of the albedo IR is rejected, the operating temperature difference decreases, increasing the PR difference up to ~10%$_{abs}$ under a desert location.

The use of ARC on glass helps to improve the *PR*, but it also can increase its thermal dependence and the operating module temperature. This PR improvement depends on how high the series resistance and the output current are; thereby any optical cell-to-module (CTM) gain would not be necessary translated in a yield gain. This evidences the need to change the module architecture or interconnection layout in order to avoid the series electrical power loss, even for terrestrial application.

For the experiment with white albedo it can be concluded that the electrical power loss are not the main module temperature driver but the sunlight irradiance, the albedo and ambient temperature play an important role, for modules located in desert locations. Setting up the ground conditions to avoid IR reflections and to increase the albedo in the visible wavelengths seems to be worthy to apply in non-polar desert locations; the module temperature could decrease, increasing the performance and reliability.

It is recommended to put attention to the glass type used for module manufacturing, because if the ARC is not tuned to reflect the IR irradiation then it will not bring the expected yield benefices. In other words, a module manufactured with an anti-reflective coated glass has more field potential if the ARC is tuned to reject the incoming infrared. Of course a detailed economical analysis must be conducted considering glass cost differences and even soiling, abrasion and wind speed effects.

Acknowledgements

This work was supported by the German Ministry of Education and Research (BMBF) under contract number CHL13WTZ-008 (SolarChilD, Solare Kollaboration zwischen Chile und Deutschland). The authors want to thank the Energy Development Centre of the University of Antofagasta, Chile, for the provided dataset and to our colleges L. J. Koduvelikulathu , H. Chu and E. Wefringhaus for the fruitful discussions.

References

[1] Bengt Perers, Simon Furbo, Jiangong Han, Weiqian Kong, Stamoulis Stergiakis. Long term testing and evaluation of PV modules with and without Sunarc antireflective coating of the cover glass. Energy Procedia 2015; 70:311-317. doi: 10.1016/j.egypro.2015.02.128.

[2] A. Cuevas, A. Luque, J. Eguren, J. del Alamo. 50 per cent more output power from an albedo-collenting flat panel using bifacial solar cells. Sol. Energy. 1982; 29:419-420.

[3] L. Kreinin, N. Bordin, A. Karsenty, A. Drori, D. Grobgeld, Y. Eisenberg. PV module power gain due to bifacial design. Preliminary experimental and simulation data. Proceedings of 35th IEEE PV Spec. Conf. 2010; pp: 2171-2175.

[4] J. P. Singh, T. M. Walsh, A. G. Aberle. Performance investigation of bifacial PV modules in the tropics. Proceedings of 27th EU-PVSEC. 2012; pp: 3263-3266.

[5] J. A. Coakley. Reflectance and albedo, surface. Encyclopedia of the Atmosphere. J.R. Holton and J.A. Curry, Eds. Academic Press. pp. 1914-1923.

[6] Rob W. Andrews, Joshua M. Pearce. The effect of spectral albedo on amorphous silicon and crystalline silicon solar photovoltaic device performance. Sol. Energy 2013; 91:233-241. doi: 10.1016/j.solener.2013.01.030.

[7] M.P. Brennan, A.L. Abramase, R.W. Andrews, J.M. Pearce. Effects of spectral albedo on solar photovoltaic devices. Sol Energy Mater Sol Cells. 2014; 124:111-116.

[8] A.M. Baldridge, S.J. Hook, C.I. Grove, G. Rivera. The ASTER spectral library version 2.0. Remote Sens. Environ. 2009. 113:711-715. doi:10.1016/j.rse.2008.11.007.

[9] Malte R. Vogt, Hendrik Holst, Matthias Winter, Rolf Brendel, Pietro P. Altermatt. Numerical modeling of c-Si PV modules by coupling the semiconductor with the thermal conduction, convection and radiation equations. Energy Procedia 2015; 77:215-224. doi: 10.1016/j.egypro.2015.07.030.

[10] IEC 61724 Std. Photovoltaic System Performance Monitoring-Guidelines for Measurements, Data Exchange and Analysis. IEC, 1998.

[11] Achim Woyte, Mauricio Richter, David Moser, Stefan Mau, Nils Reich, Ulrike Jahn. Monitoring of Photovoltaic Systems: Good Practices and Systematic Analysis. Proceedings of the 28th EU-PVSEC, Paris, France, 2013; pp: 3686-3694. doi: 10.4229/28thEUPVSEC2013-5CO.6.1.

[12] D.H. Neuhaus, R. Mehnert, G. Erfurt, M. Eberspächer, C. Hofbauer et al. Loss analysis of solar modules by comparison of IV measurements and prediction from IV curves of individual solar cells. Proceedings of the 20th EU-PVSEC, Barcelona, Spain, 2005; pp: 1947-1952.

[13] Ingrid Haedrich, Ulrich Eitner, Martin Wiese, Harry Wirth. Unified methodology for determining CTM ratios: Systematic prediction of module power. Sol Energy Mater Sol Cells. 2014; 131:14-23.

[14] J. Rabanal-Arabach, A. Schneider, E. Cabrera, R. Kopecek. Minimization of electrical losses of PV modules located in places with high solar irradiance. Proceedings of the 31st EU-PVSEC, Hamburg, Germany, 2015; pp: 2435-2438. doi: 10.4229/EUPVSEC20152015-5BV.4.15.

[15] Jai Prakash Singh, Siyu Guo, Ian Marius Peters, Armin G. Aberle, Timothy M. Walsh. Comparison of Glass/Glass and Glass/Backsheet PV modules using bifacial silicon solar cells. IEEE J-PV. 2015;5(3):783-790.
[16] Avi Braun, Eugene A. Katz, Jeffrey M. Gordon . Basic aspects of the temperature coefficients of concentrator solar cell performance parameters. Prog. Photovolt: Res. Appl. 2013; 21:1087-1094. doi: 10.1002/pip.2210.
[17] Martin Wolf, Hans Rauschenbach. Series resistance effects on solar cell measuremenst. VDI Bericht. 1963; 3:455-479.
[18] Priyanka Singh, S.N. Singh, M. Lal, M. Husain. Temperature dependence of I-V characteristics and performance parameters of silicon solar cell. Sol Energy Mater Sol Cells. 2008; 92:1611-1616.
[19] Firoz Khan, S.N. Singh, H. Husain. Effect of illumination intensity on cell parameters of a silicon solar cell. Sol Energy Mater Sol Cells. 2010; 94(9):1473-1476. doi: 10.1016/j.solmat.2010.03.018.
[20] Jens Müller, David Hinken, Susanne Blankemeyer, Heike Kohlenberg, Ulrike Sonntag, Karsten Bothe et al. Resistive power loss analysis of PV modules made from halved 15.6×15.6 cm² Silicon PERC solar cells with efficiencies up to 20.0%. IEEE J-PV. 2015; 5(1):189-194. doi: 10.1109/JPHOTOV.2014.2367868.